Available online at www.sciencedirect.com
SCIENCE DIRECT
Surface Science 600 (2006) 1860–1869
SURFACE SCIENCE
www.elsevier.com/locate/susc

Finite temperature quantum distribution of hydrogen adsorbate on nickel (0 0 1) surface

Markku Leino *, Jouko Nieminen, Tapio T. Rantala

Institute of Physics, Tampere University of Technology, P.O. Box 692, FI–33101 Tampere, Finland

Received 27 December 2005; accepted for publication 10 February 2006
Available online 3 March 2006

Abstract

Finite temperature quantum behavior of hydrogen and deuterium adsorbates on Ni(0 0 1) surface has been simulated using path-integral Monte Carlo technique. The adsorbate–surface interaction is described by the many-body alloy potential form, fitted to the adsorption parameters from DFT calculations. This allows consideration of substrate atom dynamics. Temperatures 100 K and 300 K have been considered and contribution of the thermal motion of Ni surface atoms is analyzed.

At low temperatures the quantum delocalization of the adsorbate is considerable, and therefore, temperature dependence of distributions is weak. In this case, the isotope effect is larger. At higher temperatures, however, the thermal dynamics of the substrate dominates all studied phenomena and classical description may be sufficient. By using a semi-classical description of the hydrogen adsorbate temperature dependence of the distributions and energetics becomes strong at all temperatures, providing that quantum description is necessary for the correct picture of H/Ni(0 0 1) system.

Keywords: Monte Carlo simulations; Nickel; Hydrogen atom

1. Introduction

Quantum behavior of H adsorbate on Ni and other metal surfaces has been of interest both experimentally [1,2] and theoretically [3–13]. It has been used to explain peculiar adsorbate diffusion [3–10], vibrational observations [3], electron-energy loss spectra [11,12], low-energy electron diffraction [11,12], photoemission [12], helium scattering [13], thermal desorption [4], linear optical diffraction [2] and field emission [1,2]. Most of the interesting quantum states relate to Ni(0 0 1) surface, where H adsorbate is known to delocalize and develop a two-dimensional band structure.

Quantum mechanical tunneling of a hydrogen atom between adjacent binding sites dominates diffusion at low temperatures, which is revealed by the fact that the diffusion constant is temperature independent [1–10,14]. The usual method for considering the temperature dependence of the diffusion constant from theoretical point of view is the path-centroid formulation, as proposed by Gillan [15,16], and further developed by Voth et al. [17,18]. Mattsson et al. has applied it widely [7–9]. Also quantum mechanical transition state theory [3,13,19] has been in extensive use in studies of hydrogen diffusion on a nickel surface.

The impurities of lattice, vacancies, other defects, relaxations or reconstructions, and most importantly at higher temperatures, the thermal motion of the surface need to be taken into account in studies of real surfaces [20–23]. Thus, for theoretical studies an accurate model for the interatomic interactions is required. Pair potentials cannot be expected to be successful. Therefore, several more sophisticated model potentials have been proposed, including semi-empirical potentials, embedded atom model, effective medium theory but also ab initio calculations for the

* Corresponding author. Tel.: +358 50 363 8659; fax: +358 3 3115 2600.
E-mail addresses: Markku.Leino@tut.fi (M. Leino), Tapio.Rantala@tut.fi (T.T. Rantala).

0039-6028/$ - see front matter © 2006 Elsevier B.V. All rights reserved.
doi:10.1016/j.susc.2006.02.017

potential energy surfaces have been carried out [6,7,10–12,15,24,25].

Furthermore, the complexity of hydrogen behavior on a nickel surface arises from the explicit involvement of dissipative forces due to phonons and other forms of excitations, defects, and strong interaction between the hydrogen and metal atoms. Only a few theoretical methods are capable of treating these problems.

We adopt the many-body alloy (MBA) potential [26] derived from tight-binding theory as a starting point for the adsorbate–surface interaction. It offers a possibility for extensions to description of both adsorbate–adsorbate interactions and metal surface dynamics at the finite temperature. Here, we first make the parametrization and assess the quality of resulting potential against chemisorption energies of ab initio DFT calculations and the spectroscopic observations mentioned above.

We then report fully quantum mechanical and thermally averaged constant temperature simulation of hydrogen atom on a rigid Ni(1 0 0) surface using path-integral Monte Carlo (PIMC) technique [27]. It implicitly includes thermal averaging over the quantum states of the hydrogen. Thus, we obtain the equilibrium energetics that is not provided by the path-centroid method used for evaluation of the diffusion constant. Next, we include the dynamics of the substrate nickel atoms. The thermal dynamics of Ni surface is taken into account classically and simulated with Metropolis Monte Carlo method (MMC).

Thus, we combine the PIMC for the H atom and MMC for Ni atoms into the same simulation to evaluate the finite temperature density matrix and the related distributions for the quantum adsorbed hydrogen under the influence of thermally distributed Ni surface atoms. We compare the results to the semi-classical "atoms at the adsorption sites" picture. We assess the quantum nature and temperature dependencies of the hydrogen distribution and differences with the semi-classical picture. We also consider the isotope effect by comparing distributions of hydrogen to those of deuterium.

This report is organized as follows. Section 2 describes the many-body alloy potential, in Section 3 is the path-integral formalism described, and the results are given in the Section 4. Finally, Section 5 collects the conclusions.

2. Many-body alloy potential

The analytical form of the many-body alloy potential is based on the tight-binding formalism [26,28] of bulk materials. The needed parameters can be fitted to ab initio or experimental data. It suits well for both single component and alloy bulk materials. It has been used for H/Pd systems and for studies of the electronic and structural properties of small clusters [29,30], surfaces of metals, and dilute metal alloys [28, and references therein]. Whether the same set of parameters is useful for different configurations—dimers, surfaces, bulk etc.—must be checked separately in each case.

The total (cohesive) energy of a crystal or a cluster is decomposed [26] into individual atomic contributions E_i as

$$E_{\mathrm{T}} = \sum_i E_i, \tag{1}$$

where i runs over all atoms in the system and

$$E_i = -\sqrt{\sum_{j\neq i} \xi_{\alpha\beta}^2 \exp\left[-2q_{\alpha\beta}\left(\frac{r_{ij}}{r_{0,\alpha\beta}}-1\right)\right]} + \sum_{j\neq i} \epsilon_{\alpha\beta} \exp\left[-p_{\alpha\beta}\left(\frac{r_{ij}}{r_{0,\alpha\beta}}-1\right)\right]. \tag{2}$$

The attractive part (first term) is due to the hybridization of orbitals. It is based on a parameterized tight-binding Hamiltonian and the second-moment approximation. The repulsive part (second term) is parameterized as a pair-wise Born–Mayer potential with an exponential distance dependence [26].

The parameters are defined for atom pairs (i,j) of elements α and β. Five parameters for each different pair are needed. These are the attraction due to overlapping orbitals $\xi_{\alpha\beta}$ and the pair-wise repulsion energy $\epsilon_{\alpha\beta}$, both given at the equilibrium distance $r_{0,\alpha\beta}$. The distance dependence of attractive and repulsive parts are scaled by the parameters $p_{\alpha\beta}$ and $q_{\alpha\beta}$, respectively.

Next, we consider the parameters for hydrogen on nickel. The parameters used for Ni–Ni interactions are fitted to bulk properties, and H–Ni parameters fitted to adsorption properties. General principles based on atom pair interactions and bulk cohesion are outlined in Appendix A.

2.1. Ni–Ni bulk

First, we discuss the interaction between metal atoms, since they are needed in fitting the H–Ni parameters to the adsorption data. The fitting can be done to bulk properties, for which we use the following data [31]: $a = 3.52$ Å, $r_0 = 2.49$ Å, $E_{\mathrm{coh}} = -4.44$ eV and $B = 1.17$ eV/Å^3. In addition, the coordination number in the fcc lattice is $z = 12$.

Since this set of data still leaves us with one free parameter, we utilize the Sutton–Chen parameterization to start with [31] (see Appendix A). The scaling parameter for attraction is $m = 6$, which corresponds to $q = 3.0$. Using this value for q and bulk fitting, we obtain $p = 8.6197$, $\xi = 1.9659$ eV and $\epsilon = 0.1975$ eV.

2.2. Fitting H–Ni

We attempt to fit the H/Ni(0 0 1) MBA potential to the data given by Mattsson et al. [10], where adsorption of H on Ni(0 0 1) surface has been studied with an EMT-type model potential whose parameters are fitted to ab initio potential energy surface. The fitted quantities are the adsorption energy of the hollow site, $E_{\mathrm{ads}} = 2.8$ eV, the equilibrium distance from the surface at hollow site $r_{\mathrm{a}} = 0.5$ Å and the energy barrier between the hollow sites through the bridge site, $E_{\mathrm{barr}} = 0.14$ eV, see Ref. [10].

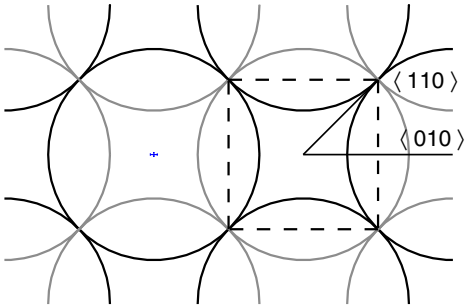

Fig. 1. Nickel (001) surface (of FCC lattice, $a = 3.52$ Å) schematically, surface and sub-surface layer atoms indicated by black and grey circles, respectively. The 4-fold hollow site is designated by the dashed square. The high-symmetry directions $\langle 010\rangle$ and $\langle 110\rangle$ along the surface are also shown. The RMS displacements related to the Ni atom thermal motion at the two temperatures, are also indicated on the left, see text.

This fitting gives parameters $q = 2.8698$, $p = 5.8659$, $r_0 = 1.4400$ Å, $\epsilon = 2.7006$ eV and $\xi = 5.5201$ eV. These give exact values for the chosen adsorption properties, but rather useless values for the dissociation energy ($E_d = 5.6390$ eV) and the force constant of the HNi molecule ($k = 45.7780$ eV/Å^2); the ab initio calculations [32] give $E_d = 3.1$ eV, $r_0 = 1.47$ Å and $k = 13.67$ eV/Å^2. Thus, fitting the surface properties leads to a parameterization that does not describe satisfactorily the HNi molecule.

2.3. H/Ni(001) model

The (001) surface of fcc nickel is illustrated in Fig. 1. The most relevant region for hydrogen adsorption is the 4-fold hollow site and the bridge site that presents the barrier between the adjacent hollow sites. The H and D distributions are given for the region depicted in Fig. 1.

In the present model consisting of N atoms, we have one quantum mechanically behaving hydrogen adsorbate on a surface of $N-1$ classical nickel atoms at either zero or at finite temperature. We take N large enough to give the hydrogen energetics from Eqs. (1) and (2) on an infinite Ni substrate. The hydrogen cut-off radius for MBA potential is essentially 8 Å, corresponding to $N \approx 100$.

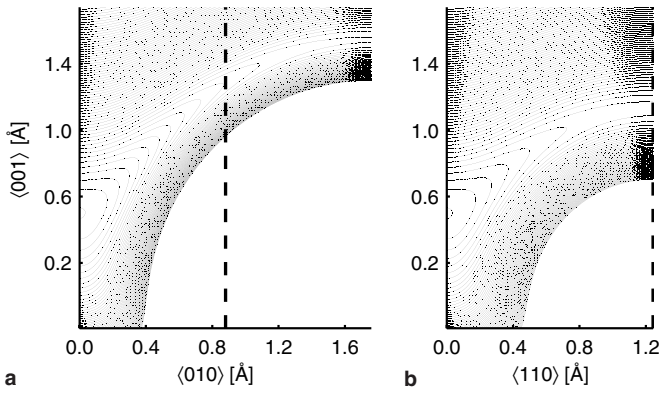

Fig. 2. Equipotential contour lines of the H atom MBA potential energy hypersurface in two surface perpendicular planes of rigid (001) surface of Fig. 1 from the hollow site to (a) the top site direction $\langle 010\rangle$ and (b) the bridge site direction $\langle 110\rangle$. The minimum at $z = 0.5$ Å corresponds to the adsorption energy 2.8 eV and line spacing is 25 meV.

It should be noted that the Ni surface seen by the hydrogen atom is perfectly periodical in two dimensions, expect for the thermal motion of Ni atoms. For nickel atom dynamics some finite-size effects may remain as a compromise with computational labour.

Fig. 2 shows the hydrogen equipotential curves at zero temperature in two high-symmetry planes perpendicular to the surface. Potential to the $\langle 110\rangle$ direction is identical with that of Mattsson et al. [10]. We see that the topsite barrier between hollow sites is about a double (0.3 eV) of that of the bridge site (0.14 eV).

3. Path-integral Monte Carlo method

All stationary properties of a quantum system with Hamiltonian $\widehat{H} = \widehat{T} + \widehat{V}$ in thermal equilibrium at temperature $\beta \equiv 1/k_B T$ are obtained from the density matrix $Z = \mathrm{Tr}\, e^{\beta \widehat{H}}$ [33]. Here, $\widehat{T} = \sum_{i=1}^{N} \hat{\mathbf{p}}_i^2/2m_i$ is the kinetic energy operator and $\widehat{V}$ includes the external potential and interactions between the quantum particles.

Obviously, quantum statistics is not important for nickel atoms at high temperatures. Even at $T = 100$ K the thermal wavelength [27] $\Lambda_\beta = (\hbar^2\beta/m)^{1/2} \approx 0.01$ Å is negligible compared to the interatomic spacing, 2.4 Å. Thus, the quantum statistics of nickel atoms becomes important only at sub-Kelvin temperatures.

3.1. Path-integral formalism

In the discrete path-integral representation partition function Z is the trace of the density matrix $\rho(\mathbf{r}', \mathbf{r})$ of one quantum particle in a d-dimensional space, given by

$$Z = \left(\frac{mM}{2\pi\hbar^2\beta}\right)^{d/2} \int \exp\left[-\beta \sum_{n=1}^{M} (K_n + U_n)\right] \mathrm{d}\mathbf{r}_0 \cdots \mathrm{d}\mathbf{r}_{M-1}, \tag{3}$$

where functions K_n and U_n define internal and external energies of the system. In the primitive approximation [27] they are written as

$$K_n = \frac{mM}{2\hbar^2\beta^2} (\mathbf{r}_{n-1} - \mathbf{r}_n)^2 \tag{4a}$$

and

$$U_n = \frac{1}{2M} (V(\mathbf{r}_{n-1}) + V(\mathbf{r}_n)), \tag{4b}$$

where m is the mass of the particle and M is called the Trotter number, and the periodic boundary conditions in imaginary time are taken into use, i.e. $\mathbf{r}_0 = \mathbf{r}_M$. The primitive approximation, where the external energy coincides with classical potential energy of the distribution, contains all the physics and converges to the correct limit, given a small enough β/M [27]. Furthermore, it is simple and well

defined, and at the limit $M \to \infty$ the exact many-body description of quantum system is obtained.

It is straightforward to calculate scalar operators, such as density and potential energy; they are simply averages over the path [27]. Use can be made of the symmetry in imaginary time, since all time slices n are equivalent. Thus, the average one-particle density is

$$\rho(\mathbf{r}) = N_\rho \sum_{i=1}^{N} \sum_{n=1}^{M} \delta(\mathbf{r} - \mathbf{r}_{i,n}), \tag{5}$$

where $\rho(\mathbf{r})$ is the diagonal part of the density matrix, $\rho(\mathbf{r}) = \rho(\mathbf{r},\mathbf{r})$, and N_ρ is a proper normalization factor for the total number of particles. N should be large enough for good sampling of the phase space at the temperature $T = 1/k_B\beta$.

The nondiagonal properties in coordinate basis, such as the energy, free energy, and momentum distribution, are not so straightforward to evaluate. The thermodynamic estimator of the energy is obtained by differentiating the partition function with respect to the inverse temperature [27] as

$$E_T(\beta) = -\frac{1}{Z}\frac{dZ}{d\beta} = M\langle dN/(2\beta) - K_n + U_n/M\rangle,$$

but this is not a useful estimator because of large fluctuations and statistical noise. Total energy can be approximated more accurately by using the virial theorem for kinetic energy

$$T_{vir}(\beta) = \tfrac{1}{2}\langle \mathbf{r}\cdot\nabla V(\mathbf{r})\rangle \tag{6}$$

and by calculating the potential energy by a scalar operator

$$E_{pot}(\beta) = \langle V(\mathbf{r})\rangle, \tag{7}$$

where the averages $\langle\cdot\rangle$ are evaluated with the density $\rho(\mathbf{r})$ as a weight function. The total energy is a sum of the two, $E_{tot}(\beta) = E_{pot}(\beta) + T_{vir}(\beta)$.

Path-integral Monte Carlo (PIMC) simulation method is a "formally exact" finite temperature approach for a quantum particle, the only limiting factor in accuracy being the computational capacity, for evaluation of the density matrix (3).

3.2. Monte Carlo simulation procedure

Conventionally, the Metropolis Monte Carlo scheme is used to evaluate the integral (3). With this technique all the approximations in the integration scheme and in path-integral formulation are controllable. The Metropolis algorithm samples effectively the one-particle distribution, and thus, the partition function Z using the integrand in (3) as the weight for the importance sampling process. The main issue is whether the configuration space is explored thoroughly in a reasonable amount of computing time. Inclusion of several types of Monte Carlo moves makes the algorithm more robust, since before calculation one does not necessarily know which type of moves will lead to a balanced sampling of the phase space and rapid convergence of expectation values. Therefore, we have used two types of moves: Some for one randomly selected "knot of the path", and another for the center-of-mass of the path.

Distribution of steps in the phase space was taken to be Gaussian such that the total Metropolis acceptance rate is about 40% and the frequency of each different type of move is about the same. This is called the *classic rule* [27] for sampling of the phase space.

Simulation is exact at the limit, where the Trotter number $M \to \infty$. However, usually the distributions and expectation values converge at some finite Trotter number, which depends on temperature and potential. This is clearly seen from the plots of adsorbate distribution at different Trotter numbers, and by testing the procedure for analytically solvable systems. We found sufficient convergence in our case with Trotter number $M = 64$. At 100 K this can be considered as a compromise with computational labour. The typical number of sufficient Monte Carlo steps is about 10^8.

4. Results

First, we describe the adsorbate distributions for the rigid and the finite temperature Ni surfaces, and then, we consider the energetics.

4.1. Adsorbate distributions

The hydrogen quantum distribution in the hollow site at low temperatures does not strongly depend on the actual temperature. It has been found to be rather similar to that at zero Kelvin [10–12]. We confirm the fact and illustrate it in Fig. 3 with the distributions from 100 K and 300 K. Indeed, rise of the temperature just slightly spreads out the distribution and the difference between the shown two almost vanishes.

The isotope effect in the distribution is more pronounced as seen in Fig. 4. Deuterium is clearly more localized: within the radius of 0.2 Å the probability density is higher and outside it is lower than that of hydrogen. A weak top-bridge direction difference is seen at the lower temperature, compare Fig. 4a and b, indicating that deuterium distribution is less circular or more classical, see below. Stensgaard and Jakobsen, cited in Ref. [10], have measured the spatial width $d = \sqrt{\langle x^2 + y^2\rangle}$ of deuterium on Ni(0 0 1) and found 0.20 Å in a nice agreement with our simulation.

It should be noted that the isotope effect is of quantum nature, as "classical" hydrogen and deuterium present identical distributions. The classical distribution and its temperature dependence is demonstrated in Fig. 5. It shows, first, the development of classical distribution from a delta function (a point) at 0 K to the extensive thermal distribution at 300 K, which is quite similar to that of quantum case. Second, comparison of Figs. 3 and 5 shows that the quantum delocalization is substantial, and relatively the

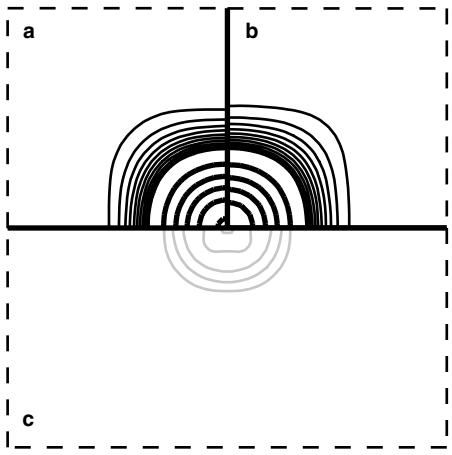

Fig. 3. Hydrogen adsorbate distributions at the hollow site of rigid substrate depicted in Fig. 1 (1.76 Å × 1.76 Å square). The equidensity contours present the three-dimensional density projected onto the surface plane, i.e., integrated over z-direction, at (a) 100 K, (b) 300 K and (c) the difference of the two ((b) − (a)). The thin and thick lines show densities $0.5, 1.0, 1.5, \ldots$ and $5, 10, 15, \ldots$ atoms/(surface unit cell); and the black and grey lines in (c) stand for positive and negative values, respectively. Here, the positive density difference is everywhere less than 0.5 atoms/(surface unit cell).

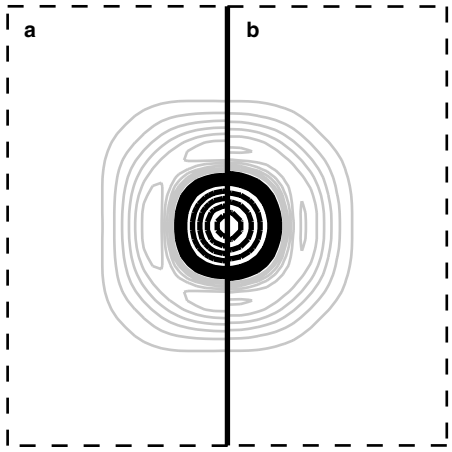

Fig. 4. Isotope effect at (a) 100 K and (b) 300 K. Differences between the deuterium and hydrogen distributions are shown, black and gray lines for positive and negative values, respectively. The equidensity curves are as defined in Fig. 3.

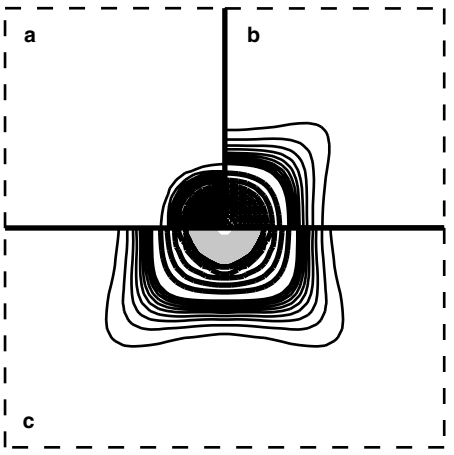

Fig. 5. The "classical hydrogen atom" distributions presented the same way as in the quantum case in Fig. 3, (a) 100 K, (b) 300 K and (c) the difference of the two ((b) − (a)).

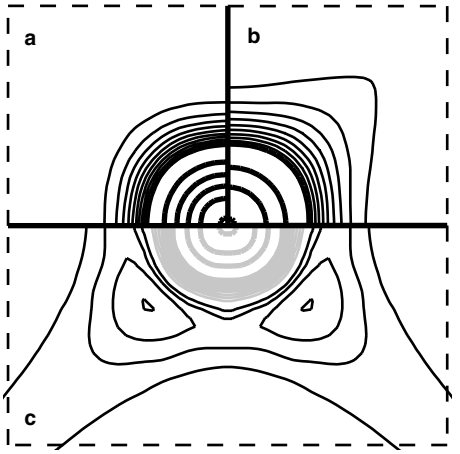

Fig. 6. The hydrogen atom distributions as in Fig. 3 but in thermal equilibrium with the same finite temperature Ni surface. Again, (a) 100 K, (b) 300 K and (c) the difference of the two ((b) − (a)).

larger the lower the temperature. We see that only at 300 K the classical thermal spreading conceals the quantum delocalization. Instead, the thermal effect on quantum delocalization in the studies of hydrogen diffusion dynamics on Ni(0 0 1) [7,8] turns on at about 40 K, already. Third, the classical distributions are more bridge direction oriented compared with the quantum case, where tunneling allows more circular shape.

Next, we consider the case of finite temperature substrate in thermal equilibrium with the adsorbate. The substrate Ni atoms are found to have thermal fluctuation around their equilibrium positions with RMS displacements 0.05 Å and 0.08 Å at the temperatures 100 K and 300 K, respectively, shown in Fig. 1. In Fig. 6 we present the consequent adsorbed hydrogen atom distributions. Though, the RMS displacements of substrate atoms do not differ too much at these temperatures, the resulting adsorbate distributions do, as seen by comparison of Figs. 3 and 6. At 100 K the distributions seem to be almost identical (Figs. a), whereas at 300 K they look clearly different (Figs. b).

Fig. 6c reveals strong temperature dependence of the distribution, that can be expected to influence on the adsorbate diffusion dynamics. Although, we have not evaluated the diffusion constants, this leads us to suggest that the temperature dependence in hydrogen diffusion on Ni(0 0 1) surface is a consequence of substrate dynamics, above 100 K. This can be contrasted with the suggestion of temperature independence arising from quantum delocalization or tunneling, below 100 K [7].

The vertical adsorbate distributions shown in Fig. 7 support the ideas and conclusions, above: On the rigid surface

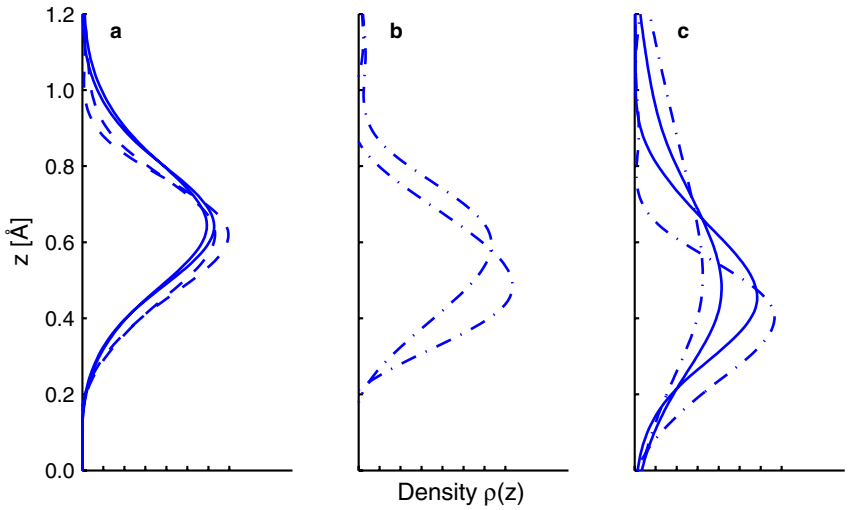

Fig. 7. Hydrogen atom distributions perpendicular to the surface, (a) quantum hydrogen (solid line) and deuterium (dashed), (b) classical hydrogen (dash-dotted) and (c) with substrate at finite temperature, hydrogen (solid line) and "classical hydrogen" (dash-dotted). All distributions are evaluated at 300 K (the one with maximum at higher z) and at 100 K (the one with maximum at lower z) temperatures.

the temperature dependence is weaker than the isotope effect, whereas it is strong for the classical adsorbate, but the largest effect on distributions arises from the finite temperature substrate dynamics in all cases. All of the vertical distributions turn out to be modified Gaussians with the width of about 0.4 Å and mean values being equal to the maxima at around 0.5–0.65 Å, except for some of the classical cases. The mean height coincides with the previously reported results, 0.6 Å [12,8].

4.2. Adsorbate energetics

Evaluation of energetics turns out to be a real computational challenge even in our case of a single quantum particle. This is due to the extremely slow convergence of statistics, although the distributions presented above have reached convergence by visual judgement. In the present case, we are able to present reliable estimates to the energy contributions in case of the rigid substrate, only.

Puska et al. [11,12] used the effective medium theory for interaction of the adsorbed hydrogen atom on Ni(0 0 1) and numerical solutions for the band structure was calculated. Mattsson et al. [8] solved the hydrogen energy levels in the ab initio DFT potential. In Table 1, a summary of these results is given. As the common basic features we can point out the lowest excited state at about 45–70 meV above the ground state and several below 100 meV.

We give the hydrogen and deuterium energetics from our PIMC simulations in Tables 2 and 3. The potential energies are referred to the bottom of the hollow site minimum. The standard error of mean is about 5 meV in all cases. Let us consider the hydrogen adsorbate first.

The potential energies are found to be about 85 meV and 90 meV for the two temperatures 100 K and 300 K, respectively. The corresponding kinetic energies evaluated from the virial formula are given as 95 meV and 100 meV, yielding the total energies as 180 meV and 190 meV. We find that our mixed state total energies are higher than those evaluated from the data in Table 1, properly weighting with the temperature. Thus, we note that the energies found here are higher than the barrier 140 meV at the bridge site between two adjacent hollow sites. But this is true for the quantum hydrogen, only, as the classical hydrogen energies, see Table 2, are 50 meV and 100 meV at 100 K and 300 K, respectively.

Table 1
Hydrogen atom energy "levels" on Ni(0 0 1) surface from the band structure calculations of Puska et al. [12] and Mattsson et al. [8] referred to the ground state

	A_1^0	A_1^1	E^1	E^2	A_1^2	100 K	300 K
Puska et al. (band center)	0	62	45	80	95	0.6	27
Mattsson et al. (Γ)	0		68		86	0.06	11

The energies are given in meV. The energy difference between potential minimum and ground state is 121 meV for Mattsson's data. The thermal averages, two last columns, for Puska et al. are estimated from the full data given in Ref. [12], including levels of B_1 and B_2 symmetry below 100 meV, whereas for Mattsson et al. only the data given in this table is used.

Table 2
Energetics for hydrogen on a rigid Ni(0 0 1) surface

	$T = 100$ K		$T = 300$ K		
	Classical	Quantum	Classical	Quantum	
Mattsson et al. [8]		121		132	E_{tot}
PIMC	25	85	49	91	E_{pot}
	24	95	48	102	T_{vir}
	49	179	97	193	E_{tot}
$\frac{3}{2}k_BT$	12.9		38.8		

All energies are given in meV.

Table 3
Energetics for deuterium

	$T = 100$ K		$T = 300$ K		
	Classical	Quantum	Classical	Quantum	
Mattsson et al. [8]		84		99	E_{tot}
PIMC	22	60	48	69	E_{pot}
	23	70	49	76	E_{kin}
	45	130	97	145	E_{tot}

HO-energetics at $\omega = \sqrt{k/m}$, thus $\sqrt{2}\omega_D = \omega_H$. All energies are given in meV.

Table 4
Energetics of hydrogen on thermally vibrating Ni surface

	$T = 100$ K		$T = 300$ K		
	Classical	Quantum	Classical	Quantum	
PIMC	116	160	330	276	E_{pot}
	208	207	578	524	E_{kin}
	324	367	908	800	E_{tot}

All energies are given in meV.

The PIMC potential and kinetic energies are relatively close to each other in both cases pointing to the harmonic oscillator like potential. The energies we obtain are close to those of a simple three-dimensional harmonic oscillator with $\hbar\omega = 120$ meV. The quantum mechanical total energy of harmonic oscillator is $\langle E\rangle = \frac{3\hbar\omega}{2}\coth\frac{1}{2}\hbar\omega\beta$, giving energies of 180 meV and 183 meV at temperatures 100 K and 300 K, respectively, when applied to this system. However, the potential is flat in all directions at its minimum with smaller force constants, $\hbar\omega$ below 100 meV.

The shape of the hollow potential and the excited state structure can be further analyzed by noting that we find the difference in the total energies in the two temperatures to be about 10 meV. This is what can be estimated from the data of Mattsson et al., as well, indicating that our potential function produce similar level structure. The absolute values, however, differ significantly, theirs being closer to the average of our classical and quantum energies. Overall, our potential is more confined at the hollow site than the one in Ref. [8]. This explains the difference of about 50 meV in the absolute values in Table 2. This also explains the difference between the classical and quantum case in Table 2: The confinement pushes the quantum hydrogen to higher potential energy region, see Fig. 7.

At this point, it is also instructive to remind about the classical simple harmonic oscillator energetics that is given independent of harmonic force constant by $\frac{3}{2}k_BT + \frac{3}{2}k_BT = 3k_BT = 26$ meV and 78 meV for the considered temperatures 100 K and 300 K, respectively.

For the deuterium we obtain 60 meV and 70 meV for potential energies, 70 meV and 75 meV for kinetic energies, and finally, 130 meV and 145 meV for the total energies in the two temperatures 100 K and 300 K, respectively. Thus, we nicely find the scaling down of energies in the quantum case by a factor $\sqrt{2}$. The difference in classical H and D reflect the statistical error, as these should be equal with large enough statistics.

Finally, we can briefly consider the energetics of hydrogen adsorbate on thermally fluctuating Ni surface. There, from the adsorbate-contribution-only calculation for the expression $E_{pot} + E_{kin} = E_{tot}$ we find $0.15\,\text{eV} + 0.2\,\text{eV} = 0.35\,\text{eV}$ and $0.3\,\text{eV} + 0.5\,\text{eV} = 0.8\,\text{eV}$ for the quantum hydrogen at 100 K and 300 K, respectively. In these cases, the classical hydrogen adsorbate takes on essentially the same energetics. This gives further support to our suggestion of the role of substrate dynamics in the temperature dependence of the adsorbate diffusion, and also, the classical nature of adsorbate properties at room temperature (Table 4).

5. Conclusions

We have carried out a study of hydrogen quantum delocalization on Ni(0 0 1) surface at finite temperatures. Adsorbate distributions and energetics were determined in two temperatures, 100 K and 300 K, to trace the temperature dependencies, and deuterium was considered to find the isotope effect. The finite temperature quantum and classical hydrogen adsorbates were considered both on a rigid substrate and one in thermal equilibrium with the adsorbate.

To flexibly describe the adsorbate–substrate interaction and those between substrate atoms we use the tight binding derived many-body alloy (MBA) potential, which contains only a few parameters. The parameters were fitted to the adsorption energetics and geometries from DFT calculations. The fit was shown to be perfect for the considered H/Ni(0 0 1) case, but lacking the universality to describe the extreme case of HNi molecule.

By comparing MBA to Sutton–Chen potential, we find that the two potentials have a one-to-one correspondence. The terms of the potentials can be attributed to different functional forms of hopping integrals in tight-binding formalism and it is possible to derive a unique connection between the parameter sets of these two.

Path-integral Monte Carlo method is shown to be straightforward but computationally intensive approach to find the finite temperature mixed quantum state even for a single particle. Also, the 0 K quantum state can be obtained as an extrapolation from finite temperatures, only, and time dependent dynamics cannot be assessed, either. On the other hand, the classical limit can be nicely found within the same formalism.

On the rigid Ni surface, we find strong quantum delocalization of the adsorbate at 100 K, the classical adsorbate being significantly more localized in terms of distribution and energetics. The 100 K mixed state energy turns out be larger than the bridge site barrier between the hollow sites. As this is obviously true down to 0 K, as well, it can be expected to be an important factor in surface diffusion dynamics.

At room temperature the extent of classical distribution approaches to that of quantum case, but a clear difference in energetics remains, 100 meV compared to 190 meV. The corresponding simple harmonic oscillator energy is 78 meV indicating the difference (or similarity) of the adsorbate potential and harmonic potential.

The isotope effect is, as expected, localization of the distributions and scaling down the energetics by a factor of $\sqrt{2}$.

The finite temperature surface dynamics seems to effect only little on distribution of the quantum adsorbate at 100 K. The energies increase somewhat, however. At room temperature the case is different, the substrate dynamics has a clear effect on both as compared to the rigid surface case. Furthermore, the substrate atom dynamics seems to make the strongest contribution to the temperature dependence of the H/Ni(0 0 1) system properties and phenomena considered here.

Acknowledgements

For financial support we thank Graduate School of Tampere University of Technology and the Academy of Finland, and for computational resources CSC, Center of Scientific Computing, Finland.

Appendix A. General aspects in MBA potential parameter fitting

Let us consider a cluster with N atoms, each of which with a coordination number z. If the equilibrium distance of the nearest neighbours is r_0, the total cohesive energy of the N-cluster from the MBA potential (1) and (2) is

$$E_N = N(-\sqrt{z}\xi + z\epsilon). \tag{A.1}$$

If we remove one atom and assume no relaxation of the cluster, there is one atom without neighbours, z atoms with a coordination number $z-1$, and $N-(z+1)$ atoms with a coordination number z. Thus, the energy of a $(N-1)$-cluster is

$$E_{N-1} = (N-(z+1))(-\sqrt{z}\xi + z\epsilon) + z(-\sqrt{z-1}\xi + (z-1)\epsilon). \tag{A.2}$$

Thus, by neglecting the lattice relaxation *the defect formation energy* is

$$\Delta E = E_N - E_{N-1} = -((1+z)\sqrt{z} - z\sqrt{z-1})\xi + 2z\epsilon. \tag{A.3}$$

It is useful to consider the limits of this result. For a pair of atoms, the defect formation energy is the same as the dissociation energy. In this case, $z=1$ and $\Delta E = -2\xi + 2\epsilon$.

In the limit of large coordination, i.e., $z \gg 1$, we find that $(z-1)^{1/2} \approx \sqrt{z}(1-1/(2z))$ and after some algebra we find $\Delta E \approx -\frac{3}{2}\sqrt{z}\xi + 2z\epsilon$.

In order to obtain *the cohesion energy,* we must allow relaxations, and assume that after removing one atom, all the remaining atoms in the $(N-1)$-cluster have a coordination number z. Hence the energy is

$$E_{N-1} = (N-1)(-\sqrt{z}\xi + z\epsilon) \tag{A.4}$$

and the cohesion energy is

$$\Delta E = E_N - E_{N-1} = -\sqrt{z}\xi + z\epsilon, \tag{A.5}$$

and this is the formula to be used in fitting parameters to the cohesion energy.

A.1. Fitting to dimer properties

Let us consider a pair of atoms with an equilibrium distance r_0. The total binding energy from (1) and (2) for the pair is

$$E_T(r) = -2\xi \exp\left[-q\left(\frac{r}{r_0}-1\right)\right] + 2\epsilon \exp\left[-p\left(\frac{r}{r_0}-1\right)\right]. \tag{A.6}$$

This couples the two energy parameters to the dissociation energy:

$$E_T(r_0) = -E_d = -2\xi + 2\epsilon. \tag{A.7}$$

The first derivative of the energy E_T at r_0 gives the condition for the equilibrium distance. This yields

$$q\xi = p\epsilon. \tag{A.8}$$

The second derivative at the r_0 is the harmonic force constant

$$k = \left.\frac{\partial^2 E_T}{\partial r^2}\right|_{r_0} = -2\left(\frac{q}{r_0}\right)^2\xi + 2\left(\frac{p}{r_0}\right)^2\epsilon. \tag{A.9}$$

Thus, given the equilibrium bond length r_0, dissociation energy E_d and harmonic force constant k, the four parameters are bound by three equations

$$\begin{aligned} pq &= \frac{kr_0^2}{E_d}, \\ \xi &= \frac{E_d}{2(p-q)}p, \\ \epsilon &= \frac{E_d}{2(p-q)}q, \end{aligned} \tag{A.10}$$

leaving one of the parameters free. Obviously, one free parameter cannot be expected to be sufficient to fit the adsorption data.

A.2. Fitting parameters to bulk properties

For bulk fitting, it is useful to scale the bond lengths as $r_{ij} = xr_0$, or $V = x^3V_0$. This transforms the equation for the energy to a form which is independent from the equilibrium bond length:

$$E_T = N\left(-\sqrt{z}\xi\exp(-q(x-1)) + z\epsilon\exp(-p(x-1))\right).$$

Since the equilibrium is obtained at $x = 1$, the total energy is

$$E_T = N(-\sqrt{z}\xi + z\epsilon). \tag{A.11}$$

Naturally, the cohesion energy is

$$E_{coh} = E_T/N = -\sqrt{z}\xi + z\epsilon.$$

Now the equilibrium condition is obtained from the derivative with respect to the scaling factor x, and it gives a condition

$$q\xi = \sqrt{z}p\epsilon. \tag{A.12}$$

A third condition is obtained from the bulk modulus

$$B = V\left.\frac{\partial^2 E_T}{\partial V^2}\right|_{r_0}.$$

We will need the following three results:

$$\left.\frac{\partial E_T}{\partial x}\right|_{r_0} = 0,\ \left.\frac{\partial^2 E_T}{\partial x^2}\right|_{r_0} = N(-\sqrt{z}q^2\xi + zp^2\epsilon),\ \text{and}$$

$$\frac{\partial V}{\partial x} = 3x^2 V_0.$$

Those results are used in the following lines

$$\frac{\partial E_T}{\partial V} = \frac{\partial x}{\partial V}\frac{\partial E_T}{\partial x} = \frac{1}{3x^2 V_0}\frac{\partial E_T}{\partial x}$$

and

$$\left.\frac{\partial^2 E_T}{\partial V^2}\right|_{r_0} = \left(\frac{1}{3x^2 V_0}\right)^2 \frac{\partial^2 E_T}{\partial x^2}.$$

Thus the bulk modulus is

$$B = \frac{N}{9V}(-\sqrt{z}q^2\xi + zp^2\epsilon).$$

This can be further simplified for fcc-crystals which have a density $N/V = a^3/4$ and thus

$$B = \frac{4}{9a^3}(-\sqrt{z}q^2\xi + zp^2\epsilon). \tag{A.13}$$

In the same way as for the pair, we obtain conditions:

$$\begin{aligned} pq &= -\frac{9Ba^3}{4E_{coh}}, \\ \xi &= -\frac{E_{coh}}{\sqrt{z}(p-q)}p, \\ \epsilon &= -\frac{E_{coh}}{z(p-q)}q. \end{aligned} \tag{A.14}$$

A.3. Comparison to Sutton–Chen potential

Sutton–Chen potential (SCP) is of the Finnis–Sinclair family, and also derived using tight-binding arguments. It can be written as a sum of cohesion energies of single atoms:

$$E_T = \sum_i E_i,$$

where

$$E_i = -\epsilon c_i \sqrt{\sum_{j\neq i}\left(\frac{r_0}{r_{ij}}\right)^m} + \frac{1}{2}\sum_{j\neq i}\epsilon\left(\frac{r_0}{r_{ij}}\right)^n.$$

Thus there is an apparent resemblance between MBA and SCP.

It is easy to show that at the limit $r_{ij} \to r_0$, there exists a more definite correspondence. Noticing that

$$\exp\left[-a\left(\frac{r_{ij}}{r_0} - 1\right)\right] = \left(\exp\left[\frac{r_{ij}}{r_0} - 1\right]\right)^{-a} \approx \left(\frac{r_0}{r_{ij}}\right)^a,$$

as $r_{ij} \approx r_0$, MBA has an approximate form

$$E_c(i) \approx -\xi\sqrt{\sum_{j\neq i}\left(\frac{r_0}{r_{ij}}\right)^{2q}} + \sum_{j\neq i}\epsilon\left(\frac{r_0}{r_{ij}}\right)^p.$$

Thus there we have a correspondence

$p \to n$
$2q \to m$
$\xi^2 r_0^{2q} \to (\epsilon c_i)^2 a^m$
$2\epsilon r_0^p \to \epsilon a^n$

For *Ni*, the SCP-parameters are $m = 6$, $n = 9$, $\epsilon = 1.5707 \times 10^{-2}$ eV, $c_i = 39.432$ and $a = 3.52$ Å. In terms of MBA, this would correspond to $q = 3.0$ and $p = 9.0$. If we choose the nearest neighbour distance for $r_0 = 2.49$ Å, the remaining parameters would be $\epsilon = 0.1771$ eV and $\xi = 1.752$ eV. As is shown in the text, the choice $q = 3.0$ and bulk fitting for MBA gives the parameters: $q = 3.0$ and $p = 8.6197$, $r_0 = 2.49$ Å, $\epsilon = 0.1975$ eV and $\xi = 1.9659$ eV. The difference between the two sets of parameters is due to different second derivative of the potential at the equilibrium position. In simulations, we utilize the latter set of parameters.

References

[1] A. Lee, X.D. Zhu, L. Deng, Phys. Rev. B 46 (23) (1992) 15472.
[2] X.D. Zhu, A. Lee, A. Wong, U. Linke, Phys. Rev. Lett. 68 (12) (1992) 1862.
[3] B.M. Rice, B.C. Garrett, M.L. Koszykowski, S.M. Foiles, M.S. Daw, J. Chem. Phys. 92 (1990) 775.
[4] S.E. Wonchoba, W.-P. Hu, D.G. Truhlar, Phys. Rev. B 51 (15) (1995) 9985.
[5] L.Y. Chen, S.C. Ying, Phys. Rev. Lett. 73 (5) (1994) 700.
[6] S. Badescu, S.C. Ying, T. Ala-Nissilä, Phys. Rev. Lett. 86 (22) (2001) 5092.
[7] T.R. Mattsson, U. Engberg, G. Wahnström, Phys. Rev. Lett. 71 (16) (1993) 2615.
[8] T.R. Mattsson, G. Wahnström, Phys. Rev. B 31 (3) (1995) 1885.
[9] T. Mattsson, G. Wahnström, Phys. Rev. B 56 (23) (1997) 14944.
[10] T. Mattsson, G. Wahnström, L. Bengtsson, B. Hammer, Phys. Rev. B 56 (1997) 2258.
[11] M.J. Puska, R.M. Nieminen, M. Manninen, B. Chakraborty, S. Holloway, J.K. Nørskov, Phys. Rev. Lett. 51 (1983) 1081.
[12] M.J. Puska, R.M. Nieminen, Surf. Sci. 157 (1985) 413.
[13] S.W. Rick, D.L. Lynch, J.D. Doll, J. Chem. Phys. 99 (10) (1993) 8183.
[14] K.A. Muttalib, J. Sethna, Phys. Rev. B 32 (6) (1985) 3462.

[15] M.J. Gillan, Phys. Rev. Lett. 58 (6) (1987) 563.
[16] M.J. Gillan, J. Phys. C 20 (1987) 3621.
[17] G.A. Voth, D. Chandler, W.H. Miller, J. Phys. Chem. 93 (1989) 7009.
[18] G.A. Voth, D. Chandler, W.H. Miller, J. Chem. Phys. 12 (1989) 7749.
[19] Y.-C. Sun, G.A. Voth, J. Chem. Phys. 98 (9) (1993) 7451.
[20] M.S. Daw, M.I. Baskes, Phys. Rev. B 29 (1984) 6443.
[21] P. Jena, R.M. Nieminen, M.J. Puska, M. Manninen, Phys. Rev. B 31 (12) (1985) 7612.
[22] M.J. Puska, R.M. Nieminen, P. Jena, Phys. Rev. B 35 (12) (1987) 6059.
[23] K.F.F. Assa Auerbach, R. Gomer, J. Chem. Phys. 86 (4) (1987) 2356.
[24] G. Mills, H. Jónsson, Phys. Rev. Lett. 72 (7) (1994) 1124.
[25] J.K. Nørskov, J. Chem. Phys. 12 (1989) 7461.
[26] W.Z.Y.S. Li, D. Tománek, Phys. Rev. B 44 (23) (1991) 13053.
[27] D.M. Ceperley, Rev. Mod. Phys. 67 (2) (1995) 279.
[28] W. Zhong, Y. Cai, D. Tománek, Phys. Rev. B 46 (1992) 8099.
[29] H. Grönbeck, D. Tománek, S.G. Kim, A. Rosén, Chem. Phys. Lett. 264 (1997) 39.
[30] H. Grönbeck, D. Tománek, S.G. Kim, A. Rosén, Z. Phys. D 40 (1997) 469.
[31] A. Sutton, J. Chen, Philos. Mag. Lett. 61 (3) (1990) 139.
[32] P. Bagus, C. Björkman, Phys. Rev. A 23 (1981) 461.
[33] R.P. Feynman, Statistical Mechanics, Addison-Wesley, 1972, 1988.